Real-Time Nuclear Magnetic Resonance Detection of Fumarase Activity Using Parahydrogen-Hyperpolarized [1-13C]Fumarate

Real Time Nuclear Magnetic Resonance Detection of Fumarase Activity using Parahydrogen-Hyperpolarized [1-^{13}C]fumarate

James Eills[a,*], Eleonora Cavallari[b], Carla Carrera[c], Dmitry Budker[a,d], Silvio Aime[b], and Francesca Reineri[b]

a) Helmholtz Institute, Johannes Gutenberg University, Mainz, Germany, b) Dept. of Molecular Biotechnology and Health Sciences, University of Torino, Torino, Italy c) Institute of Biostructures and Bioimaging, National Research Council of Italy, Torino, Italy d) Department of Physics, University of California, Berkeley, U.S.A., (*) Corresponding author. Email: eills@uni-mainz.de

Abstract

Hyperpolarized fumarate can be used as a probe of real-time metabolism in vivo, using carbon-13 magnetic resonance imaging. Dissolution dynamic nuclear polarization is commonly used to produce hyperpolarized fumarate, but a cheaper and faster alternative is to produce hyperpolarized fumarate via PHIP (parahydrogen induced polarization). In this work we *trans*-hydrogenate [1-^{13}C]acetylene dicarboxylate with *para*-enriched hydrogen using a commercially available Ru catalyst in water to produce hyperpolarized [1-^{13}C]fumarate. We show that fumarate is produced in 89% yield, with succinate as a side product in 11% yield. The proton polarization is converted into ^{13}C magnetization using a constant adiabaticity field cycle, and a polarization level of 24% is achieved using 86% *para*-enriched hydrogen gas. We inject the hyperpolarized [1-^{13}C]fumarate into cell suspensions and track the metabolism. This work opens the path to greatly accelerated preclinical studies using fumarate as a biomarker.

Introduction

MRI (magnetic resonance imaging) is a powerful, noninvasive medical technique, but has limitations due to the intrinsic low sensitivity. To overcome this problem, it is possible to hyperpolarize the nuclear spins, a procedure that has been shown to produce signal enhancements of biomolecules up to 10^5 at high field [1,2]. Unfortunately, the hyperpolarization decays on a timescale of up to several minutes due to nuclear spin relaxation [3,4]. Despite this temporal limitation, it is possible to observe real-time cellular metabolism in vitro and in vivo after injection of hyperpolarized metabolites [5-8].

One promising candidate metabolite is [1,4-$^{13}C_2$]fumarate, which is converted to [1,4-$^{13}C_2$]malate by the enzyme fumarase in one step of the citric acid cycle. Fumarate transport through the cell membrane is a relatively slow process, and so significant formation of malate is only observed in regions of necrotic cells where fumarate has access to the enzyme. This change in chemical identity can be observed in carbon-13 MRI via CSI (chemical shift imaging), and has been shown to be a sensitive marker of cell necrosis [9-11]. The technique is currently being assessed for application in clinical trials [6] which opens exciting new possibilities for imaging of cell necrosis and diagnostics of therapeutic response [11,12]. All in vivo experiments to date have used [1,4-$^{13}C_2$]fumarate polarized via dDNP (dissolution dynamic nuclear polarization) [13]. There are three significant drawbacks to this technique [14]: (1) it is prohibitively expensive, (2) complex cryogenic equipment is required to reach 1.4 K, and (3) the hyperpolarized material is delivered in batch-mode with tens of minutes of preparation time required between sample deliveries. The recently developed 'large dose dDNP' [15], and 'bullet DNP' [16] techniques might help to overcome the final point.

PHIP (parahydrogen induced polarization) is an alternative hyperpolarization modality which involves chemical addition of hydrogen gas enriched in the *para* spin isomer to a substrate molecule [2,17]. PHIP is approximately 1-2 orders of magnitude less expensive than dDNP, and can produce hyperpolarized products with a much higher duty cycle because it only requires chemical reaction with hydrogen gas [18,19]. However, the application of this powerful tool to in vivo metabolic studies has been limited to a few metabolites that can be hyperpolarized via parahydrogen addition to an unsaturated precursor of the target molecule [20-24], although the use of several biomolecules has been demonstrated in vivo [25-30]. Hyperpolarized [1-^{13}C]fumarate has been recently obtained from the pairwise addition of parahydrogen to [1-^{13}C]acetylene dicarboxylate, thanks to the use of a *trans*-hydrogenative Ru-based catalyst (Fig. 1) [31]. This represents a significant development, because the most widely used hydrogenative PHIP catalyst (a Rh-based complex) leads to *cis*-hydrogenation of substrates, and its use here would lead to toxic maleate being obtained [32]. However, in order to progress to meaningful metabolic application, it is crucial to improve the fumarate polarization level and yield of the hydrogenation reaction.

In this work the unsaturated precursor molecule [1-^{13}C]acetylene dicarboxylate at a concentration of 50 mM in D_2O was completely hydrogenated with parahydrogen (86% enriched) at 80°C and a pressure of 9.6 bar in a high-pressure NMR tube to produce [1-^{13}C]fumarate. D_2O is used (rather than H_2O) to extend the lifetime of the nuclear spin order. After reaction, the protons are initially hyperpolarized in a nonmagnetic 'singlet state' [33]. In our experiment, the proton singlet order was transformed into hyperpolarized magnetization on the 1-^{13}C spin by subjecting the sample to a magnetic field cycle [34-37]. Here we used a 'constant adiabaticity' [38] field-cycling profile, which means the applied field as a function of time has been optimized to give maximum polarization transfer for any given duration (see Supporting Information for details). The chemical reaction and magnetic field cycle profile are shown in Fig. 1.

Results

To measure the polarization achieved on the hydrogenated substrate, the NMR tube used for the reaction was placed into the high field magnet immediately after the field cycle for acquisition of a hyperpolarized NMR spectrum. The time between the end of the field cycle and signal acquisition was 20 ± 2 s. After the hyperpolarized NMR signal had fully relaxed, a 512 transient thermal equilibrium spectrum was acquired with a 92 s recycle delay between transients. A comparison between the hyperpolarized and thermal equilibrium spectra is shown in Fig. 2. The ^{13}C T_1 was measured to be 26 ± 1 s, and taking into account the recycle delay used for acquisition of the thermal signal, the signal enhancement factor was calculated to be 20,000 at 14.1 T, corresponding to a polarization level of 24%. The ratio of peak integrals between fumarate and succinate in the thermal spectrum indicates 89% fumarate yield (45 mM), and 11% succinate yield (5 mM), and there is no detectable unreacted starting material. We have set an upper bound on the concentration of unreacted starting material at <0.4 mM. The succinate is thought to be produced from fumarate reacting with dissolved hydrogen.

To study PHIP-polarized fumarate as a probe of cellular necrosis, experiments were performed in which the reaction mixture containing hyperpolarized [1-^{13}C]fumarate was added to cell suspensions. Three experiments were performed; one in which the cell media contained 10 million lysed EL-4 tumour cells, one with 10 million intact (healthy) EL-4 tumour cells, and one with no cells in the media. In these experiments, after perfusion of the [1-^{13}C]fumarate containing solution through the cells suspension, the ^{13}C NMR signal was acquired every 2 s using 15° flip-angle pulses, so as to probe the metabolism over time without significantly perturbing the magnetization.

From the control experiment without cells in the media, and after applying a correction for signal decay due to continual rf pulsing [39], the fumarate T_1 under our experimental conditions was A stack plot of the ^{13}C NMR spectra for the two experiments carried out in the presence of cells is shown in Fig. 3. In the experiment with intact cells, fumarate transport across the cell membrane is slow relative to T_1, so no malate signal is detected. In the experiment with lysed cells, the fumarate has access to the enzyme and reacts with water to form malate. The asymmetry of this molecule means the ^{13}C spin is distributed between the 1 and 4 positions, and [1-^{13}C]malate and [4-^{13}C]malate signals are observed at 181.7 and 180.5 ppm, respectively. The signal reaches a maximum at 18-20 s after the injection, and decays due to T_1 relaxation and continual rf pulsing. The [1-^{13}C]fumarate signal is at 175.4 ppm, and is significantly larger than the malate signals.

The fumarate and malate peak integrals are plotted in Fig. 4, and a fit to the data is obtained using a kinetic model that only includes fumarate conversion to malate, and relaxation of both species:

$$F \xrightarrow{k} M. \qquad (1)$$

We can write the following differential equations:

$$\frac{dF(t)}{dt} = -k\,F(t) - \frac{1}{T_x}\,F(t), \qquad (2)$$

$$\frac{dM(t)}{dt} = k\,F(t) - \frac{1}{T_x}\,M(t), \qquad (3)$$

where $F(t)$ is the time-dependent concentration of hyperpolarized [1-^{13}C]fumarate, $M(t)$ is the time-dependent concentration of hyperpolarized [1-^{13}C]malate and [4-^{13}C]malate, and k is the forward reaction-rate constant. In this model, for simplicity we assume that both species relax with the same time constant T_x, which is a combination of T_1 and the signal decay due to successive pulses. T_x is known from the [1-^{13}C]fumarate measurement discussed above, and the rate constant k was treated as a fitting parameter. This model yielded k = 1.62 ± 0.01 x 10^{-3} s^{-1}. Including a rate

constant for the reverse reaction did not improve the quality of the fit. We note that the measured rate constant is higher than has been previously reported [11]. This may be due to a difference in the experimental conditions; specifically, a higher cell concentration was used in this work.

Discussion

To explain the dramatic increase in ^{13}C polarization over the original demonstration (2% ^{13}C polarization, using 50% *para*-enriched hydrogen) [31], we consider the key experimental differences. Importantly, we have an improvement in the polarization level by a factor of 2.4 by using 86% *para*-enriched hydrogen gas instead of the 50% used previously, since the polarization level is proportional to $(4f-1)/3$, where f is the *para*-enrichment level of the gas. In the previously reported experiments, the hydrogenation reaction took 30 s and was performed by bubbling hydrogen gas into a reaction solution at 50 °C in the high field NMR magnet. In the present case, the reaction was faster (10 s), and was carried out by shaking the sample at 80°C in Earth's magnetic field (~50 μT). Firstly, by using a shorter reaction time in this work, there was less time for nuclear spin relaxation to occur. Secondly, it is possible that parahydrogen singlet order is lost due to singlet/triplet mixing occurring on the reaction intermediates [40]; this destructive process is likely to be more efficient at high magnetic field due to larger chemical shift differences between the parahydrogen protons on the reaction intermediates. Thirdly, longer hydrogenation times may lead to partial degradation of the catalyst, with formation of metal-containing species which may enhance the rate of parahydrogen relaxation. It should also be considered that the reaction solution in the previous work was likely not at 50°C as expected, because the bubbling of room-temperature hydrogen gas would lower the reaction temperature.

In previous studies employing dDNP as the polarization technique, the doubly ^{13}C-labelled isotopomer [1,4-$^{13}C_2$]fumarate was used. Here, the [1-^{13}C] isotopomer was used, which means the maximum achievable ^{13}C signal is lower by a factor of 2. There are unitary bounds on the achievable polarization transfer from proton singlet order into ^{13}C magnetization, which depend on the symmetry of the spin system [41]. Assuming an initial state of pure proton singlet order, the maximum possible transfer into X-spin (^{13}C) polarization for the [1-^{13}C] isotopomer, an AA'X spin system (Pople notation), is 1, corresponding to 100% ^{13}C polarization. However, for the [1,4-$^{13}C_2$] isotopomer, an AA'XX' spin system, the ^{13}C polarization of each is limited to 50%. This therefore gives the same observable ^{13}C signal enhancement as using the [1-^{13}C] isotopomer. This limitation cannot be overcome without further reducing the symmetry of the spin system. It could still be beneficial to use the [1,4-$^{13}C_2$] isotopomer, because the relaxation properties of the spins should differ based on the symmetry, which might yield higher overall signal enhancements.

The NMR measurements were carried out at 14.1 T, and the fumarate 1-^{13}C T_1 was 28 ± 1 s. The T_1 is longer at lower field because the dominant relaxation mechanism is chemical shift anisotropy [42], and a fumarate ^{13}C T_1 of 58 ± 2 s has been reported at a field of 3 T [43]. The T_1 does not increase far beyond this value at lower fields, presumably because another relaxation mechanism becomes dominant (e.g. dipole-dipole relaxation from coupling to the nearby protons). A T_1 of ~60 s can be expected in applications of [1-^{13}C]fumarate in clinical imaging scanners, which typically employ field strengths of 1-3 T.

In conclusion, we have demonstrated that PHIP allows for the production of highly polarized [1-^{13}C]fumarate at a concentration of 45 mM in aqueous solution. Using relatively inexpensive and easily operated PHIP equipment, a ^{13}C polarization level of 24% was observed on [1-^{13}C]fumarate. For the reaction, we used 86% *para*-enriched hydrogen gas, meaning the polarization level could be increased to 30% by switching to 100% *para*-enriched hydrogen. Following the perfusion of lysed cells with the fumarate solution, metabolic transformation into malate was observed. Prior to application in vivo it will be necessary to extract the catalyst from the solution [44]. Unfortunately, at this time there is no toxicological information available regarding the ruthenium catalyst, and this is something we hope to investigate in the near-future. This work paves the way for accelerated preclinical studies with hyperpolarized fumarate, to better understand what role it can play in diagnostics. Whether PHIP- or dDNP-polarized fumarate will be favored for application in the clinic remains to be seen.

Materials and Methods

Cell culture

The EL-4 murine lymphoma cell line was purchased from American Type Culture Collection (ATCC) and grown in Dulbecco's Modified Eagle's Media supplemented with 10% Fetal Bovine Serum and 1 % Penicillin Streptomycin. Cells were cultured in Corning T-175 flasks at 37°C in a humidified atmosphere containing 5% CO_2. Cultures were maintained at 10^5-10^6 cells/ml by addition of fresh media every 2 days.

Hydrogenation and polarization transfer

All the chemicals were purchased from Sigma Aldrich. In a solution of 50 mM disodium [1-^{13}C]acetylene dicarboxylate and 100 mM sodium sulphite in D_2O, the ruthenium catalyst [RuCp*$(CH_3CN)_3$]PF_6 was dissolved by gentle heating and sonication. The solution was filtered using a PTFE syringe filter (Whatman UNIFLO) with 0.22 µm diameter pores, with a final catalyst concentration of 8 mM. 300 µl of the filtered solution was frozen in a 5 mm pressurisable NMR tube equipped with a J. Young valve. The tube was held in a liquid nitrogen bath (77 K) and pressurized with 2.1 bar of *para*-enriched hydrogen (86% enriched). The sample was kept at 77 K to prevent any chemical reaction before the start of the hyperpolarization experiment.

To initiate the hydrogenation reaction, the NMR tube was heated in a hot water bath at 80°C for 30 s which melted the sample and raised the internal pressure to 9.6 bar, then shaken vigorously for 10 s. The NMR tube was opened to release the parahydrogen pressure and immediately placed in a magnetic shield (Aspect Imaging, Shoham, Israel) for the application of a magnetic field cycle. The magnetic shield was used without one set of end caps, and a Mag-03 fluxgate magnetometer (Bartington, Witney, U.K.) was used to measure a 50 nT residual field inside. Magnetic fields were applied using a solenoid coil controlled by a Keysight Technologies 33220A 20 MHz waveform generator (Keysight Technologies, Santa Rosa, U.S.). The field was initially set at 1.5 mT, dropped to 50 nT in less than 1 ms, then increased adiabatically to 3.7 µT in 4 s (see Fig. 1). The sample was then removed from the shield for NMR experiments.

NMR experiments were performed at 14.1 T in a 5 mm BBO probe using a Bruker AVANCE console. In the experiment to obtain the ^{13}C polarization level, spectra were acquired of the hyperpolarized reaction mixture every 2 s using 5° flip-angle pulses. After this, a thermal equilibrium spectrum of the sample was acquired with 512 transients, using 90° flip-angle pulses separated by 90 s intervals.

Cell suspension experiments

After hydrogenation of the 300 µl sample and magnetic field cycle, the hyperpolarized reaction mixture was collected in a syringe containing 150 µl of acidic buffer solution (HEPES 144 mM, pH 5.5) to produce a 450 µl solution with physiological osmolarity (290 ± 2 mOsm) and optimal pH (7.6 ± 0.2) for the enzyme activity. 200 µl of the hyperpolarized reaction mixture was injected into a 5 mm NMR tube via syringe through PTFE tubing (1.6 mm O.D., 0.8 mm I.D.) in the high field NMR magnet. The NMR tube contained 200 µl of culture media at 37°C. The sample temperature was 34 ± 5 °C upon arrival in the magnet, and equilibrated at 37°C in a few seconds. The time between the end of the field cycle and the first signal acquisition was 28 ± 5 s.

The EL-4 tumour cells were counted using a Burker chamber, centrifuged in the growth media for 5 min at 125x g-force, and the supernatant was removed. 10.0 ± 0.1 million cells were suspended in 200 µl of culture media and transferred into a 5 mm NMR test tube for experiments. For experiments on lysed cells, this cell suspension was double freeze-thawed in liquid nitrogen. The NMR tube (containing either lysed or intact cells) was then placed in the NMR magnet and equilibrated at 310 K. At the end of each experiment the number of cells was quantified using a Bradford protein assay with a specific calibration line, and was measured to be 10 ± 0.1 million in all experiments.

Acknowledgements

This project has received funding from the European Union's Horizon 2020 research and innovation program under the Marie Skłodowska-Curie Grant Agreement No. 766402, and Compagnia di San Paolo (Athenaeum Research 2016, n. CSTO164550). The authors would like to thank Bogdan Rodin for calculating the constant adiabaticity field-cycling profile, and Christian Bengs for invaluable help running experiments.

References

[1] Nikolaou, P.; Goodson, B. M.; and Chekmenev, E. Y.; NMR hyperpolarization techniques for biomedicine, *Chem. Eur. J.* **2015**, 21, 3156-3166

[2] Green, R. A.; Adams, R. W.; Duckett, S. B.; Mewis, R. E.; Williamson, D. C.; Green, G. G. R.; The theory and practice of hyperpolarization in magnetic resonance using parahydrogen, *P. Nucl. Mag. Res. Sp.* **2012**, 67, 1-48

[3] McCormick, J.; Korchak, S.; Mamone, S.; Ertas, Y. N.; Liu, Z.; Verlinsky, L.; Wagner, S.; Glöggler, S.; Bouchard, L.-S.; More Than 12 % Polarization and 20 Minute Lifetime of 15N in a Choline Derivative Utilizing Parahydrogen and a Rhodium Nanocatalyst in Water, *Angew. Chem. Int. Ed.* **2018**, 57, 10692-10696

[4] Shchepin, R. V.; Birchall, J. R.; Chukanov, N. V.; Kovtunov, K. V.; Koptyug, I. V.; Theis, T.; Warren, W. S.; Gelovani, J. G.; Goodson, B. M.; Shokouhi, S.; Rosen, M. S.; Yen, Y.-F.; Pham, W.; Chekmenev, E. Y.; Hyperpolarizing Concentrated Metronidazole 15NO2 Group over Six Chemical Bonds with More than 15% Polarization and a 20 Minute Lifetime, *Chem. Eur. J.* **2019**, 25, 8829-8836
[5] Wang, Z. J.; Ohliger, M. A.; Larson, P. E. Z.; Gordon, J. W.; Bok, R. A.; Slater, J.; Villanueva-Meyer, J. E.; Hess, C. P.; Kurhanewicz, J.; Vigneron, D. B.; Hyperpolarized ^{13}C MRI: State of the Art and Future Directions, *Radiology* **2019**, 291, 273-284
[6] Kurhanewicz, J.; Vigneron, D. B.; Ardenkjaer-Larsen, J. H.; Bankson, J. A.; Brindle, K.; Cunningham, C. H.; Gallagher, F. A.; Keshari, K. R.; Kjaer, A.; Laustsen, C.; Mankoff, D. A.; Merritt, M. E.; Nelson, S. J.; Pauly, J. M.; Lee, P.; Ronen, S.; Tyler, D. J.; Rajan, S. S.; Spielman, D. M.; Wald, L.; Zhang, X.; Malloy, C. R.; Rizi, R.; Hyperpolarized ^{13}C MRI: Path to Clinical Translation in Oncology, *Neoplasia* **2019**, 21, 1-16
[7] Nelson, S. J.; Kurhanewicz, J.; Vigneron, D. B.; Larson, P. E. Z.; Harzstark, A. L.; Ferrone, M.; van Criekinge, M.; Chang, J. W.; Bok, R.; Park, I.; Reed, G.; Carvajal, L.; Small, E. J.; Munster, P.; Weinberg, V. K.; Ardenkjaer-Larsen, J. H.; Chen, A. P.; Hurd, R. E.; Odegardstuen, L. I.; Robb, F. J.; Tropp, J.; Murray, J. A.; Metabolic imaging of patients with prostate cancer using hyperpolarized [1-^{13}C] pyruvate, *Sci. Transl. Med.* **2013**, 5, 198ra108-198ra108
[8] Cavallari, E.; Carrera, C.; Sorge, M.; Bonne, G.; Muchir, A.; Aime, S.; Reineri, F.; The ^{13}C hyperpolarized pyruvate generated by parahydrogen detects the response of the heart to altered metabolism in real time, *Sci. Rep.* **2018**, 8, 8366-8375
[9] Clatworthy, M. R.; Kettunen, M. I.; Hu, D.-E.; Mathews, R. J.; Witney, T. H.; Kennedy, B. W.; Bohndiek, S. E.; Gallagher, F. A.; Jarvis, L. B.; Smith, K. G.; Brindle, K. M.; Magnetic resonance imaging with hyperpolarized [1,4-$^{13}C_2$] fumarate allows detection of early renal acute tubular necrosis, *Proc. Natl. Acad. Sci. U.S.A.* **2012**, 109, 13374-13379
[10] Miller, J. J.; Lau, A. Z.; Nielsen, P. M.; McMullen-Klein, G.; Lewis, A. J.; Jespersen, N. R.; Ball, V.; Gallagher, F. A.; Carr, C. A.; Laustsen, C.; Bøtker H. E.; Tyler D. J.; Schroeder, M. A.; Hyperpolarized [1,4-$^{13}C_2$]Fumarate Enables Magnetic Resonance-Based Imaging of Myocardial Necrosis, *JACC Cardiovasc. Imaging* **2018**, 11, 1594-1606
[11] Gallagher, F. A.; Kettunen, M. I.; Hu, D. E.; Jensen, P. R.; Zandt, R. I.; Karlsson, M.; Gisselsson, A.; Nelson, S. K.; Witney, T. H.; Bohndiek, S. E.; Hansson, G.; Peitersen, T.; Lerche, M. H.; Brindle, K. M.; Production of hyperpolarized [1,4-$^{13}C_2$] malate from [1,4-$^{13}C_2$] fumarate is a marker of cell necrosis and treatment response in tumors, *Proc. Natl. Acad. Sci. U.S.A.* **2009**, 106, 19801-19806
[12] Mignion, L.; Dutta, P.; Martinez, G. V.; Foroutan, P.; Gillies R. J.; Jordan, B. F.; Monitoring chemotherapeutic response by hyperpolarized ^{13}C-fumarate MRS and diffusion MRI, *Cancer Res.* **2014**, 74, 686–694
[13] Ardenkjaer-Larsen, J. H.; On the present and future of dissolution-DNP, *J. Magn. Reson.* **2016**, 264, 3-12
[14] Leggett, J.; Hunter, R.; Granwehr, J.; Panek, R.; Perez-Linde, A. J.; Horsewill, A. J.; McMaster, J.; Smith, G.; Köckenberger, W.; A dedicated spectrometer for dissolution DNPNMR spectroscopy, *Phys. Chem. Chem. Phys.* **2010**, 12, 5883-5892
[15] Lipso, K. W.; Bowen, S.; Rybalko, O.; Ardenkjaer-Larsen, J. H.; Large Dose Hyperpolarized Water with Dissolution-DNP at High Magnetic Field, *J. Magn. Reson.* **2017**, *274*, 65-72
[16] Kouřil, K.; Kouřilová, H.; Bartram, S.; Levitt, M. H.; Meier, B.; Scalable dissolution-dynamic nuclear polarization with rapid transfer of a polarized solid, *Nat. Commun.* **2019**, 10**,** 1733
[17] Bowers, C. R.; Weitekamp, D. P.; Parahydrogen and synthesis allow dramatically enhanced nuclear alignment, *J. Am. Chem. Soc.* **1987**, 109, 5541-5542
[18] Coffey, A. M.; Shchepin, R. V.; Feng, B.; Colon, R. D.; Wilkens, K.; Waddell, K. W.; Chekmenev, E. Y.; A pulse programmable parahydrogen polarizer using a tunable electromagnet and dual channel NMR spectrometer, *J. Magn. Reson.* **2017**, 284, 115-124
[19] Waddell, K. W.; Coffey, A. M.; Chekmenev, E. Y.; In Situ Detection of PHIP at 48 mT: Demonstration Using a Centrally Controlled Polarizer, *J. Am. Chem. Soc.* **2011**, *133*, 97-101
[20] Cavallari, E.; Carrera, C.; Reineri, F.; ParaHydrogen Hyperpolarized Substrates for Molecular Imaging Studies, *Isr. J. Chem.* **2017**, 57, 833-842
[21] Chekmenev, E. Y.; Hövener, J.; Norton, V. A.; Harris, K.; Batchelder, L. S.; Bhattacharya, P.; Ross, B. D.; Weitekamp, D. P.; PASADENA Hyperpolarization of Succinic Acid for MRI and NMR Spectroscopy, *J. Am. Chem. Soc.* **2008**, 130, 4212–4213
[22] Shchepin, R. V; Coffey, A. M.; Waddell, K. W.; Chekmenev, E. Y.; PASADENA Hyperpolarized 13C Phospholactate, *J. Am. Chem. Soc.* **2012**, 134, 3957-3960
[23] Reineri, F.; Boi, T.; Aime, S.; ParaHydrogen Induced Polarization of 13C Carboxylate Resonance in Acetate and

Pyruvate, *Nat. Commun.* **2015**, *6*, 5858
[24] Cavallari, E.; Carrera, C.; Aime, S.; Reineri, F.; 13C MR Hyperpolarization of Lactate by Using ParaHydrogen and Metabolic Transformation in Vitro, *Chem. Eur. J.* **2017**, 23, 1200-1204
[25] Zacharias, N. M.; Chan, H. R.; Sailasuta, N.; Ross, B. D.; Bhattacharya, P.; Real-Time Molecular Imaging of Tricarboxylic Acid Cycle Metabolism in Vivo by Hyperpolarized 1-13C Diethyl Succinate, *J. Am. Chem. Soc.* **2012**, 134, 934-943
[26] Zacharias, N. M.; McCullough, C. R.; Wagner, S.; Sailasuta, N.; Chan, H. R.; Lee, Y.; Hu, J.; Perman, W. H.; Henneberg, C.; Ross, B. D.; Bhattacharya, P.; Towards Real-time Metabolic Profiling of Cancer with Hyperpolarized Succinate, *J. Mol. Imaging Dyn.* **2016**, 6, 123
[27] Bhattacharya, P.; Chekmenev, E. Y.; Reynolds, W. F.; Wagner, S.; Zacharias, N.; Chan, H. R.; Bünger, R.; Ross, B. D.; Parahydrogen-induced polarization (PHIP) hyperpolarized MR receptor imaging in vivo: a pilot study of 13C imaging of atheroma in mice, *NMR Biomed.* **2011**, 24, 1023-1028
[28] Coffey, A. M.; Feldman, M. A.; Shchepin, R. V.; Barskiy, D. A.; Truong, M. L.; Pham, W.; Chekmenev, E. Y.; High-resolution hyperpolarized in vivo metabolic 13C spectroscopy at low magnetic field (48.7 mT) following murine tail-vein injection, *J. Magn. Reson.* **2017**, 281, 246-252
[29] Coffey, A. M.; Shchepin, R. V.; Truong, M. L.; Wilkens, K.; Pham, W.; Chekmenev, E. Y.; Open-Source Automated Parahydrogen Hyperpolarizer for Molecular Imaging Using 13C Metabolic Contrast Agents, *Anal. Chem.* **2016**, 88, 8279-8288
[30] Salnikov, O. G.; Shchepin, R. V.; Chukanov, N. V.; Jaigirdar, L.; Pham, W.; Kovtunov, K. V.; Koptyug, I. V.; Chekmenev, E. Y.; Effects of Deuteration of 13C-Enriched Phospholactate on Efficiency of Parahydrogen-Induced Polarization by Magnetic Field Cycling, *J. Phys. Chem. C* **2018**, 122, 24740-24749
[31] Ripka, B.; Eills, J.; Kourilova, H.; Leutzsch, M.; Levitt, M. H.; Münnemann, K.; Hyperpolarized fumarate via parahydrogen, *Chem. Commun.* **2018**, 54, 12246-12249
[32] Eills, J.; Stevanato, G.; Bengs, C.; Glöggler, S.; Elliott, S. J.; Alonso-Valdesueiro, J.; Pileio, G.; Levitt, M. H.; Singlet order conversion and parahydrogen-induced hyperpolarization of ^{13}C nuclei in near-equivalent spin systems, *J. Magn. Reson.* **2017**, 274, 163-172
[33] Levitt, M. H.; Singlet nuclear magnetic resonance, *Annu. Rev. Phys. Chem.* **2012**, 63, 89-105
[34] Jóhannesson, H.; Axelsson, O.; Karlsson, M.; Transfer of Para-Hydrogen Spin Order into Polarization by Diabatic Field Cycling. *Comptes Rendus Phys.* **2004**, 5, 315–324
[35] Cavallari, E.; Carrera, C.; Boi, T.; Aime, S.; Reineri, F.; Effects of magnetic field cycle on the polarization transfer from parahydrogen to heteronuclei through long-range *J*-couplings, *J. Phys. Chem. B* **2015**, 119, 10035-10041
[36] Golman, K.; Axelsson, O.; Johannesson, H.; Mansson, S.; Olofsson, C.; Petersson, J. S.; Parahydrogen-induced polarization in imaging: subsecond 13C angiography, *Magn. Reson. Med.* **2001**, 46, 1-5
[37] Eills, J.; Blanchard, J. W.; Wu, T.; Bengs, C.; Hollenbach, J.; Budker, D.; Levitt, M. H.; Polarization transfer via field sweeping in parahydrogen-enhanced nuclear magnetic resonance, *J. Chem. Phys.* **2019**, 150, 174202
[38] Rodin, B. A.; Sheberstov, K. F.; Kiryutin, A. S.; Hill-Cousins, J. T.; Brown, L. J.; Brown, R. C. D.; Jamain, B.; Zimmermann, H.; Sagdeev, R. Z.; Yurkovskaya, A. V.; Ivanov, K. L.; Constant-adiabaticity radiofrequency pulses for generating long-lived singlet spin states in NMR, *J. Chem. Phys.* **2019**, 150, 064201
[39] Balzan, R.; Fernandes, L.; Pidial, L.; Comment, A.; Tavitian, B.; Vasos, P. R.; Pyruvate cellular uptake and enzymatic conversion probed by dissolution DNP-NMR: the impact of overexpressed membrane transporters, *Magn. Reson. Chem.* **2017**, 55, 579-583
[40] Kating, P.; Wandelt, A.; Selke, R.; Bargon, J.; Nuclear singlet/triplet mixing during hydrogenations with parahydrogen: an in situ NMR method to investigate catalytic reaction mechanisms and their kinetics. 2. Homogeneous hydrogenation of 1,4-dihydro-1,4-epoxynaphthalene using different rhodium catalysts, *J. Phys. Chem.* **1993**, 97, 13313-13317
[41] Levitt, M. H.; Symmetry constraints on spin dynamics: Application to hyperpolarized NMR, *J. Magn. Reson.* **2016**, 262, 91-99
[42] Eills, J.; Alonso-Valdesueiro, J.; Salazar Marcano, D. E.; da Silva, J. F.; Alom, S.; Rees, G. J.; Hanna, J. V.; Carravetta, M.; Levitt, M. H.; Preservation of nuclear spin order by precipitation, *ChemPhysChem* **2018**, 19, 40-44
[43] Eldirdiri, A.; Clemmensen, A.; Bowen, S.; Kjær, A.; Ardenkjær-Larsen, J. H.; Simultaneous imaging of hyperpolarized [1,4-$^{13}C_2$]fumarate, [1-^{13}C]pyruvate and ^{18}F–FDG in a rat model of necrosis in a clinical PET/MR scanner, *NMR in Biomedicine*, 2017; 30:e3803
[44] Barskiy, D. A.; Ke, L. A.; Li, X.; Stevenson, V.; Widarman, N.; Zhang, H.; Truxal, A.; Pines, A.; Rapid Catalyst

Capture Enables Metal-Free Parahydrogen-Based Hyperpolarized Contrast Agents, *J. Phys. Chem. Lett.* **2018**, *9*, 2721– 2724

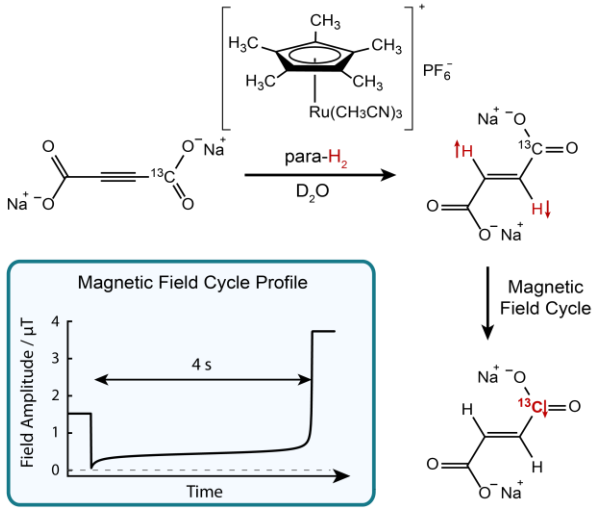

Figure 1: Reaction scheme showing the chemical addition of *para*-enriched hydrogen to an unsaturated [1-^{13}C]acetylene dicarboxylate precursor, to yield [1-^{13}C]fumarate. The proton singlet order is then transformed into ^{13}C magnetization by applying a constant-adiabaticity magnetic field cycle, optimized for the [1-^{13}C]fumarate *J*-couplings. The field-cycling profile is shown in the inset. The *J*-couplings and field-cycling profile are given in the Supporting Information.

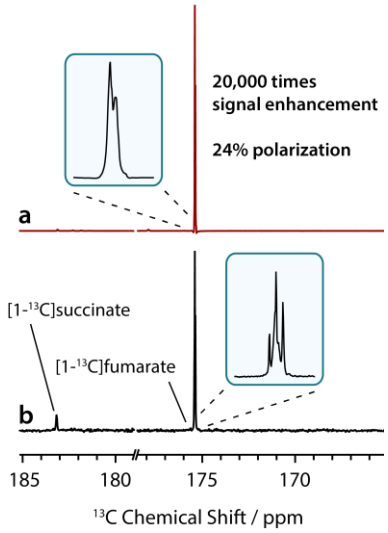

Figure 2: ^{13}C NMR spectra shown with 0.5 Hz line broadening acquired without proton decoupling. The region 178.5 to 179 ppm contained a pulse artifact and has been cut for clarity. a) A hyperpolarized spectrum of the reaction sample acquired after hydrogenation with parahydrogen, magnetic field cycle, and transport to high field. The hyperpolarized spectrum was acquired with a single transient after applying a pulse with a flip-angle of 5°. b) A thermal equilibrium spectrum of the reaction sample acquired after the hyperpolarized signals had fully relaxed. The thermal equilibrium spectrum was acquired with 512 transients using 90° flip-angle pulses, and has been vertically expanded by a factor of 4.

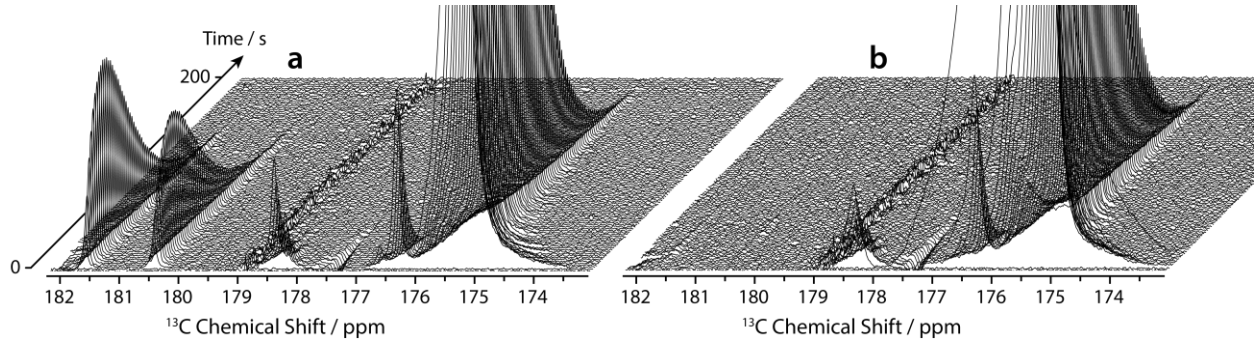

Figure 3: Hyperpolarized ^{13}C NMR spectra shown with 0.5 Hz line broadening acquired without proton decoupling. Both datasets were acquired on reaction samples after hydrogenation with parahydrogen, magnetic field cycle, and injection into a suspension of (a) lysed, and (b) intact (live) EL-4 tumour cells, at high field. Spectra were acquired every 2 s using 15° flip-angle pulses. The peaks at 175.4 ppm correspond to [1-^{13}C]fumarate, and the peaks in (a) at 180.5 and 181.7 ppm correspond to [4-^{13}C]malate and [1-^{13}C]malate, respectively. The rapidly relaxing peaks at 176.4 and 178.5 ppm are thought to be low concentration catalyst side-products.

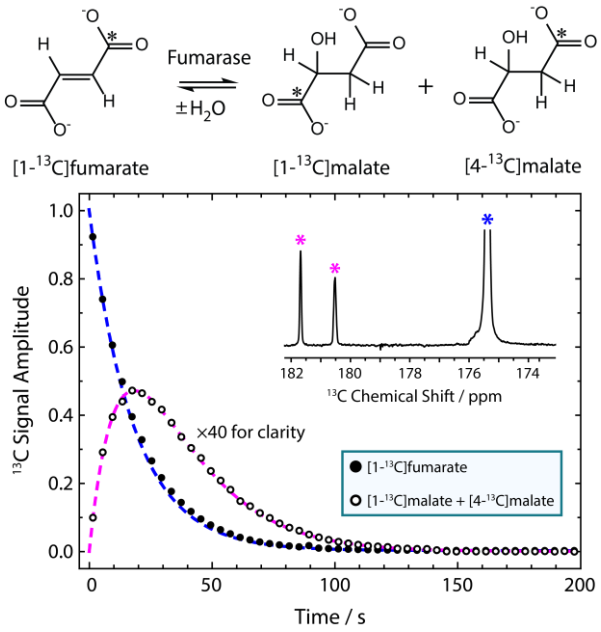

Figure 4: Top: The enzymatic conversion of [1-^{13}C]fumarate into both [1-^{13}C]malate and [4-^{13}C]malate. Bottom: Flux of ^{13}C -label between fumarate and malate in a suspension of lysed EL-4 tumour cells. The filled black dots represent integrals of [1-^{13}C]fumarate and hollow black dots represent integrals of [1-^{13}C]malate+[4-^{13}C]malate signals. The signals have been normalized, with 1 corresponding to the initial [1-^{13}C]fumarate signal. In both datasets, every other datapoint has been dropped for clarity, and the malate signal amplitude has been magnified by a factor of 40. The error bars are contained within the data points. The inset spectrum shows a single acquisition from the dataset. Fits to the data are shown by dashed blue (fumarate) and magenta (malate) lines.

TOC Figure

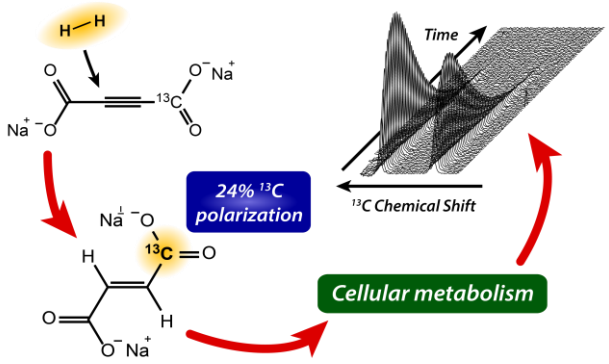
H—H
Time
24% 13C polarization
13C Chemical Shift
Cellular metabolism